A mathematical model for a rapid calculation of the urban canyon albedo and its applications

A mathematical model for a rapid calculation of the urban canyon albedo and its applications

Hongjie Zhang [a], Runming Yao [a,c] *, Qing Luo [b], Wenbo Wang [c]

[a] Joint International Research Laboratory of Green Buildings and Built Environments (Ministry of Education), Chongqing University, Chongqing, 400045, China

[b] National Centre for International Research of Low-carbon and Green Buildings (Ministry of Science and Technology), Chongqing University, Chongqing, 400045, China

[c] School of the Built Environment, University of Reading, Reading, RG6 6DF, UK

*Corresponding author: r.yao@cqu.edu.cn; r.yao@reading.ac.uk

Abstract

Urban canyon albedo (UCA) is a primary indicator used to evaluate the impact of urban geometry on radiation absorption. A rapid and effective theoretical calculation for the UCA is helpful in urban design. This research establishes a simplistic but robust mathematical model for calculating the UCA. The model was validated using prior observational studies showing that the maximum root mean square error (*RMSE*) is 0.03, and the minimum Pearson correlation coefficient (r) is 0.63. The model was then used to evaluate the influence of urban canyon geometry and materials on UCA. The results show that the canyon aspect ratio controls the UCA, especially when the canyon aspect ratio is less than 4. Furthermore, high-albedo facades can effectively increase UCA, and high-albedo pavements are recommended only if the urban canyon aspect ratio is less than 1. Finally, the solar performance of urban canyons on an urban scale was estimated by combining our model with digital elevation model (DEM) data. This study can be used in urban planning to estimate the radiation performance of an urban canyon quickly before full-scale urban thermal environment simulation.

Keywords: urban canyon albedo; multiple reflections; canyon aspect ratio; canyon orientation; urban solar radiation

Nomenclature

Symbols	
E_{ini}	Initial incoming energy on the street canyon ($\mathrm{W/m^2}$)
E_{abs}	Absorbed energy by street canyon ($\mathrm{W/m^2}$)
E_{re}	Reflected energy by street canyon ($\mathrm{W/m^2}$)
F	View factor of the street canyon to sky
$F_{z\to s}$	View factor of the sunlit area of the urban canyon to the sky
f	Cloud fraction of the target location
G_s	Solar constant ($\mathrm{W/m^2}$)
h	Height of the street canyon (m)
h_t	Hour angle (°)
I	Horizontal global solar radiation ($\mathrm{W/m^2}$)
I_d	Horizontal diffuse radiation ($\mathrm{W/m^2}$)
I_0	Horizontal extraterrestrial solar radiation ($\mathrm{W/m^2}$)
I_l	Downward atmospheric longwave radiation ($\mathrm{W/m^2}$)
I_c	Theoretical clear-sky global solar radiation of the target location ($\mathrm{W/m^2}$)
k_T	Sky cleanness coefficient
N	The day number in the year
T_a	Atmospheric temperature (K)
w	Width of the street canyon (m)
w_s	Shadow length caused by beam radiation (m)
z	Hight of walls that is directly sunlit by beam radiation (m)
Greek symbols	
$\alpha_b, \alpha_d, \alpha_l$	Effective urban canyon absorption rate of beam radiation, diffuse radiation, and downward atmospheric longwave radiation
β	Solar declination angle (rad)
ε_a	Atmospheric emissivity
θ	Solar zenith angle (rad)
$\rho_h, \rho_w\ \rho_{ave}$	Average albedo of wall, pavement, and all surfaces of street canyon
ρ_1	Average albedo of the area that is directly sunlit by beam radiation
ρ_b, ρ_d, ρ_l	Effective urban canyon albedo of beam radiation, diffuse radiation, and downward atmospheric longwave radiation
ρ_s	Effective urban canyon albedo of solar radiation
ρ_a	Effective urban canyon albedo of solar radiation and downward atmospheric longwave radiation
σ	Stefan-Boltzmann constant ($5.67\times10^{-8}\mathrm{W/m^2K^4}$)
φ_s	Solar azimuth angle (rad)
φ_c	Street canyon azimuth angle (rad)

φ_{lat}	Latitude of the target location (°)

1. Introduction

Rapid urbanization and population increase have caused a gradual deterioration in the urban thermal environment, of which the urban heat island (UHI) is one of the most prominent manifestations. The UHI affects a building's cooling load in summer, resulting in substantial increases in peak power for cooling [1,2]. In addition, the UHI causes outdoor thermal discomfort and excessive thermal stress [3], also the risk of death associated with high temperatures increases significantly [4].

Urban geometry is found to have a highly significant primary influence on the urban thermal environment [5]. First, urban morphology tends to develop vertically due to the shortage of land in urban compared to rural areas. High-density urban layouts trap the solar radiant energy through multiple reflections and reduce overall urban ventilation due to increased surface roughness [6,7]. Secondly, artificial materials (e.g., concrete, asphalt) with low albedo and high heat capacity replace natural elements (e.g., water, vegetation) [8,9]. These impermeable materials also reduce evapotranspiration, thus increasing heat accumulation in urban areas and intensifying the UHI effect [10]. Previous studies have adopted the urban albedo to evaluate the impacts of urban structure and materials on the balance of urban radiation [11,12]. Urban albedo is the ratio of the reflected radiation to the incident radiation, and it considers the multiple reflections of radiation between streets and walls [13]. Remote sensing technology is an effective method of assessing the urban albedo [14–16]. However, remote sensing methods are unsuitable for guiding urban planning since such images can only be obtained for existing urban areas.

Another important method for evaluating urban albedo is numerical calculation [17,18]. In numerical analysis, complex urban structures often need to be simplified into a generalized urban structure concept. The urban canyon is the most popular simplification of an urban structure [19–21], composed of a road with buildings on both sides. It is the most basic urban form, occupying two-thirds of a city [3]. At the same time, the concept of urban canyon albedo (UCA) was defined to represent the influence of urban structural characteristics and the albedo of the materials used on the overall urban albedo. UCA refers to the ratio of the reflected radiant energy to the radiant energy entering the urban canyon [22]. UCA demonstrates the ability of urban canyons to capture radiant energy, which is the primary indicator for evaluating the impact of

urban morphology on the urban thermal environment.

Large-scale urban construction and development have become an irresistible trend, especially in developing countries. For example, the National Bureau of Statistics estimated that the urbanization rate of China would reach 65.5% by 2050 [23]. The prediction of UCA is significant for evaluating urban radiation balance, improving the urban thermal environment, and alleviating the adverse effects of an UHI.

1.1 Existing mathematical models for calculation the effective urban canyon albedo

One of the first attempts to model urban canyon albedo came from the work of Aida and Gotoh [24]. Their model deals with solar radiation transfer with a fully two-dimensional method. That is to say, the model can only be applied to north-south street canyons in low latitudes near the equator. Nevertheless, it helps demonstrate the effect of canyon geometry on solar radiation transmission. Arnfield [25] proposed a two-dimensional urban canyon model that can handle multiple reflections inside urban canyons using the Lambertian assumption. This model is used to estimate the diurnal variation of shortwave reflection coefficients. Another early work on UCA came from Sakakibara [26], whose model processed the building shadow effect more accurately using 3-D solar angles. However, this model's main limitation is that it ignores multiple reflections within an urban canyon.

In recent years, several urban canyon radiative transfer models have been developed. Sailor and Fan developed a model in which building dimensions and spacing can be varied to simulate a more realistic urban environment [18]. In their approach, successive reflection events were valuated numerically until changes in the radiation from the canyon top drop below a specified amount between events. Qin [22] developed a similar model in which he calculated the changes in radiation absorbed by the walls and road inside the urban canyon to evaluate reflection events. Fortuniak [27] estimated UCA using a method to calculate the radiation absorbed by a facet after multiple reflections to and from other facets. Luo proposed a simple method for assessing urban albedo, but it does not consider the building shadow effect [28].

In addition, some radiative balance models can also calculate UCA. Panão *et al*. [29] developed a three-dimensional urban block radiative balance model integrating the linear equations' exact solution with Monte Carlo techniques. Yang and Li [30] developed another three-dimensional numerical model, which they used to investigate the impact of urban geometry on average urban albedo and surface temperature. The

effect of trees on radiative transfer in street canyons has also been considered. Krayenhoff *et al*. [31] established a multi-layer urban canopy model with trees using Monte Carlo ray tracing and studied the influence of trees on UCA.

The treatment of multiple reflections is the main difference between the UCA models. The most direct method is Monte Carlo ray tracing [24,29,31,32], which is usually used to deal with radiation transmission in complex environments. It requires the simulation of as many photons as possible to ensure the reliability of the results. This method is time-consuming and requires researchers to have specific coding experience. In addition, as a simulation method, Monte Carlo ray tracing can only obtain numerical solutions, which significantly limits the application of the model. Another approach is to assess the reflection events by continuous numerical calculations until the change in average irradiance occurring from the canyon top drops to a specified amount between the two events [18,22,25]. This method reduces the amount of numerical simulation, but the iterative calculation is still cumbersome, which hinders the establishment of an analytical formula for the effective reflectance of street canyons. The complexity of multiple reflections makes it difficult to obtain an analytical equation for the radiative transfer within street canyons. As far as we know, there is no relevant model to extract an effective analytical formula for the UCA.

After decades of development, the calculation model of UCA is still a complex process. None of the existing mathematical models derive a simple theoretical formula for UCA. The complexity of existing models significantly limits engineering application and the ability to couple calculations with other models, especially for the rapid assessment of urban scale solar radiation. In addition, downward atmospheric longwave radiation is usually ignored, despite being another urban energy source, especially at night.

In order to address the deficiencies mentioned above, this research aims to develop a new mathematical model that can perform a rapid calculation of UCA for the assessment of radiation performance at the neighborhood and urban scales. Such a simple model is expected to be robust and able to provide a rapid evaluation of the effect of direct and isotropic radiation on UCA.

2. Methodology

A mathematical modeling method is implemented in this study. The model includes the radiation parameters model and the UCA calculation model. The solar

radiation parameters model was set up to obtain radiation parameters such as solar position, the fraction of diffuse solar radiation, and downward atmospheric longwave radiation for locations lacking weather stations. The radiation parameters model outputs serve as inputs for the UCA calculation model relating urban geometry factors, such as view factor and multiple reflections, to simulate radiation transmission of direct and isotropic radiation in an urban canyon. This model is then validated using ideal and actual street canyon experimental data. Implementation of the model has demonstrated the practical value of the newly-developed model. The research framework is illustrated in Fig. 1.

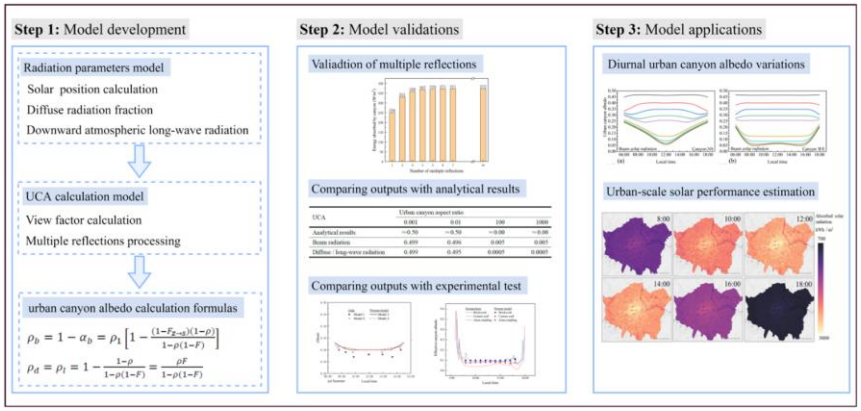

Fig. 1. The framework of this research.

2.1 Description of the mathematical model

This model makes the following three assumptions commonly used in the urban canyon model [18,22,27]. (1) The urban canyon is infinitely long and uniform. (2) All surfaces of the urban canyon are Lambertian emitters and reflectors. (3) Diffuse solar radiation and downward atmospheric longwave radiation entering the urban canyon from all-sky angles are assumed to be Lambertian radiation sources.

The geometry and angle definitions of the urban canyon are shown in Fig. 2, where θ is the solar zenith angle, φ_s is the solar azimuth angle, φ_c is the orientation of the urban canyon in which 0 denotes the north-south direction and $\pi/2$ the east-west direction, w (m) is the canyon width, h (m) is the wall height, z (m) is the height of the sunlit wall, and w_s (m) is the length of shadow in the width direction of the canyon generated by the direct radiation.

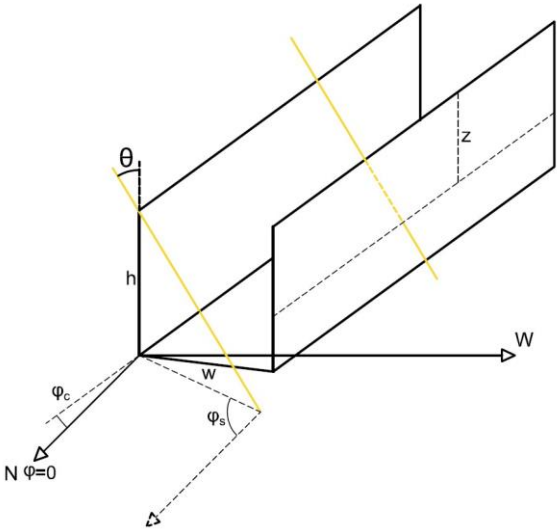

Fig. 2. Definition of urban canyon geometry and angles.

2.2 Radiation parameters model

2.2.1 Solar position

The most common method to determine the incident direction of direct solar radiation is by solar position. Generally, the solar position is determined by the solar zenith angle and solar azimuth angle. Solar position algorithms are mainly divided into fast algorithms used in engineering applications [33,34] and high-precision astronomical algorithms [35,36]. This study adopted a high-precision solar position algorithm proposed by Grena, and the detailed calculation can be found in Grena [37]. The algorithm computes the local coordinates of the sun corrected taking into account the atmospherical refraction. The solar zenith angle, θ (rad), and solar azimuth angle, φ_s (rad), are determined by [37]

$$\theta = \frac{\pi}{2} - \text{asin}(sin\varphi_{lat} sin\delta_t + cos\varphi_{lat} cos\delta_t ch_t) - \Delta e \quad (1)$$

$$\varphi_s = atan2(sh_t, ch_t sin\varphi_{lat} - tan\delta_t cos\varphi_{lat}) \quad (2)$$

where the solar azimuth angle φ_s varies from $-\pi$ to π, and the azimuth is positive in the eastern hemisphere. δ_t is the topocentric declination, φ_{lat} is the latitude, sh_t and ch_t are correlated with topocentric hour angle h_t, sh_t approximate cosine of h_t, ch_t approximate cosine of h_t, Δe is the atmospheric refraction.

2.2.2 Diffuse solar radiation

A part of solar radiation is scattered by gases, dust, aerosols, and so on, when solar radiation passes through the atmosphere. This part of solar radiation is called diffuse solar radiation. The fraction of diffuse to global solar radiation has been the subject of many models [38–41]. The Orgill and Hollands model was used in this study [42]

$$\frac{I_d}{I}=\begin{cases}1.0-0.249k_T & k_T<0.35\\ 1.557-1.84k_T & 0.35\le k_T\le 0.75\\ 0.177 & k_T>0.75\end{cases} \tag{3}$$

where I_d ($\mathrm{W/m^2}$) is the horizontal diffuse solar radiation, I ($\mathrm{W/m^2}$) is the horizontal global solar radiation, and k_T is the sky clearness coefficient; the value of k_T is given by [43]

$$k_T=\frac{I}{I_0} \tag{4}$$

where I_0 ($\mathrm{W/m^2}$) is the horizontal extraterrestrial solar radiation for a period between hour angles h_1 and h_2 (h_2 is larger). The mathematical expression is shown in Eq. (5) [44]:

$$I_0=\frac{12\times 3600G_s}{\pi}[1+0.033\cos(\frac{360N}{365})]\times\{\cos\varphi_{lat}\cos\beta(\sin h_2-\sin h_1)+[\frac{\pi(h_2-h_1)}{180}]\sin\varphi_{lat}\sin\beta\} \tag{5}$$

in which, $G_s=1366.1\ \mathrm{W/m^2}$ is the solar constant [45], φ_{lat} is the latitude, β is the solar declination angle, and is determined from Eq. (6) [22]:

$$\beta=0.409\sin(2\pi\frac{284+N}{365}) \tag{6}$$

where N is the day number in the year.

When I is not available from observations, it can be estimated from Eq. (7) [22,46]:

$$I=G_s\tau^{1/\cos\varphi_s}\cos\theta \tag{7}$$

where τ is a constant varying from 0.62 to 0.81, 0.81 for a cloudless day.

2.2.3 Downward atmospheric longwave radiation

The energy radiated downward by the atmosphere is downward atmospheric longwave radiation. The atmosphere is regarded as Lambertian in this study, and the energy is emitted uniformly into hemispherical space. A widely accepted method to estimate downward atmospheric longwave radiation under both clear and cloudy conditions was adopted in this study [47].

$$I_l=(1-f)\varepsilon_a\sigma T_a^4+f\cdot\sigma T_a^4 \tag{8}$$

where I_l (W/m^2) is the downward atmospheric longwave radiation, T_a (K) is the air temperature of the calculation layer, $\sigma = 5.67\times10^{-8} W/m^2K^4$ is the Stefan-Boltzmann constant, ε_a is the atmospheric emissivity and can be calculated by Brunt [48], f is the cloud fraction as calculated using [47]

Field Code Changed

$$f = 1 - I/I_c \quad (9)$$

where I is the global solar radiation, and I_c is the theoretical clear-sky global solar radiation under the same conditions. I_c can be calculated using the time fraction of bright sunshine and solar radiation at an extraterrestrial level [49].

2.3 UCA calculation model

Unlike the previous urban canyon albedo model [18,22,27], this study models direct solar radiation and isotropic radiation separately due to their completely different transfer paths inside the urban canyon. And the radiative transfer between four facets (one road, two walls, and the sky) is simplified to the sky and a concave surface. This method dramatically reduces the view factors and multiple reflections calculation between the various surfaces of the urban canyon. Thus, this study handles the multiple reflections in urban canyons in a simple and robust way.

2.3.1 View factor

(1) View factor calculation of direct solar radiation

There are two urban canyon exposure scenarios according to the relationship between shadow length w_s and canyon width w. First, one canyon wall is partially sunlit while the other wall and the road are shaded, as shown in Fig. 3a. Secondly, one canyon wall is fully sunlit, and the road is partially sunlit, as shown in Fig. 3b. The shadow length w_s is computed by

$$w_s = h tan\theta |\sin(\varphi_s - \varphi_c)| \quad (10)$$

Scenario 1: $w_s \geq w$, the wall is partially sunlit, and the height of the sunlit wall, z, can be calculated by

$$z = h - \frac{w_s - w}{tan\theta |\sin(\varphi_s - \varphi_c)|} \quad (11)$$

The view factor of the sunlit area of the urban canyon to the sky, $F_{z\to s}$, is

$$F_{z\to s} = \frac{z + w - \sqrt{w^2 + z^2}}{2z} \quad (12)$$

The weighted average albedo of the street canyon that is directly sunlit by solar radiation ρ_1 is

$$\rho_1 = \rho_h \quad (13)$$

where ρ_h is the albedo of the wall.

Scenario 2: $w_s < w$, one wall is fully sunlit, the height of the sunlit wall is h, the width of the sunlit road is $w - w_s$, and the view factor of the sunlit area of the urban canyon to the sky can be calculated by

$$F_{z\to s} = \frac{w}{w+h-w_s} F_{s\to z} \tag{14}$$

where $F_{s\to z}$ is the view factor of the sky to the sunlit area of the urban canyon, and $F_{s\to z}$ is

$$F_{s\to z} = 1 - \frac{w+\sqrt{h^2+{w_s}^2}-\sqrt{h^2+(w-w_s)^2}}{2w} \tag{15}$$

The weighted average albedo of the part of the urban canyon that is directly sunlit by solar radiation ρ_1 is

$$\rho_1 = \frac{h\rho_h+(w-w_s)\rho_w}{w-w_s+h} \tag{16}$$

where ρ_w is the albedo of the road.

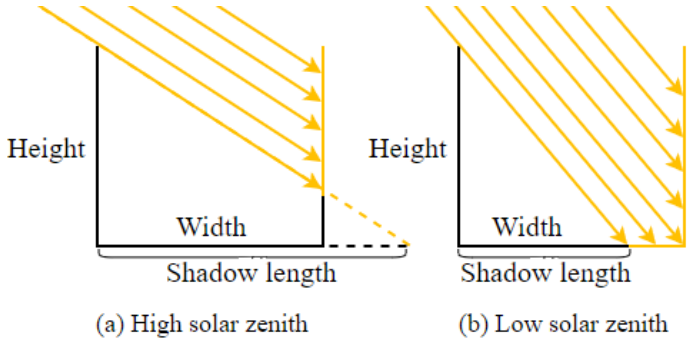

Fig. 3. Direct solar radiation received in a canyon at (a) a high and (b) a low solar zenith angle.

(2) View factor calculation of isotropic radiation

Downward atmospheric longwave radiation and diffuse solar radiation radiate uniformly to the urban canyon from the urban canyon top, assumed to be an imaginary surface, as shown in Fig. 4. The view factor of the sky to the canyon is 1. The view factor of the canyon to the sky can be calculated by

$$F = \frac{w}{w+2h} \tag{17}$$

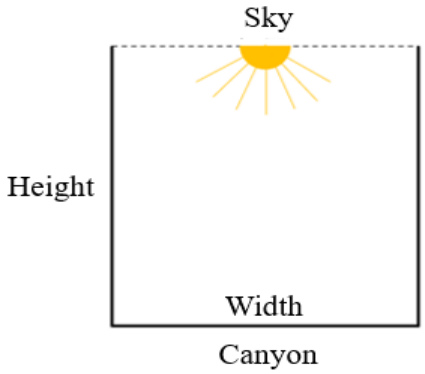

Fig. 4. Downward atmospheric longwave and diffuse solar radiation received in the urban canyon.

2.3.2 Multiple reflections

(1) Multiple reflections of direct solar radiation

This study assumes that the initial direct solar radiation entering the canyon is E_{ini} and the albedo of the first reflection is ρ_1. The photons then reflect multiple times inside the urban canyon, and the albedo of each time is the weighted average albedo ρ_{ave}, abbreviated as ρ in the following formulas, of all facets in the urban canyon. The absorbed and reflected energy of the urban canyon are E_{abs} and E_{re} , respectively.

$$\rho_{ave} = \frac{w\rho_w + 2h\rho_h}{2h+w} \quad (18)$$

where ρ_w is the albedo of the road and ρ_h is the albedo of the walls. The energy absorbed and reflected after the first reflection can be calculated as

$$E_{abs1} = E_{ini}(1-\rho_1) \quad (19a)$$

$$E_{re1} = E_{ini}\rho_1 \quad (19b)$$

The reflected energy is divided into the part radiated to the sky, $E_{ini}\rho_1 F_{z\to s}$, and the part radiated to the urban canyon, $E_{ini}\rho_1(1-F_{z\to s})$. The energy absorbed and reflected after the second reflection can be calculated as

$$E_{abs2} = E_{ini}\rho_1(1-F_{z\to s})(1-\rho) \quad (20a)$$

$$E_{re2} = E_{ini}\rho_1(1-F_{z\to s})\rho \quad (20b)$$

The reflected energy is divided into the part radiated to the sky, $E_{ini}\rho_1(1-F_{z\to s})\rho F$, and the part radiated to the urban canyon, $E_{ini}\rho_1(1-F_{z\to s})\rho(1-F)$. The energy absorbed and reflected after *n* reflections can be calculated as

$$E_{absn} = E_{ini}\rho_1\rho^{n-2}(1-F_{z\to s})(1-F)^{n-2}(1-\rho) \quad (21a)$$

$$E_{ren} = E_{ini}\rho_1\rho^{n-1}(1-F_{z\to s})(1-F)^{n-2} \quad (21b)$$

The energy absorbed by the urban canyon during all the multiple reflections is

$$
\begin{aligned}
E_{abs} &= E_{abs1} + E_{abs2} + E_{abs3} + \mathrm{L} + E_{absn} \\
&= E_{ini}(1-\rho_1) + E_{ini}\rho_1(1-F_{z\to s})(1-\rho) + \mathrm{L} + E_{ini}\rho_1\rho^{n-2}(1-F_{z\to s})(1-F)^{n-2}(1-\rho) \\
&= E_{ini}[1-\rho_1 + \frac{\rho_1(1-F_{z\to s})(1-\rho)(1-\rho^n(1-F)^n)}{1-\rho(1-F)}]
\end{aligned}
\tag{22}
$$

This study used infinite multiple reflections ($n \to \infty$) to replace the finite multiple reflections in the actual situation. The feasibility of this hypothesis was verified in section 3.1, and the above formula converges to

$$
\lim_{n\to\infty} E_{abs} = E_{ini}\left[1 - \rho_1 + \frac{\rho_1(1-F_{z\to s})(1-\rho)}{1-\rho(1-F)}\right] \tag{23}
$$

The effective absorptivity of the urban canyon for direct radiation is

$$
\alpha_b = \frac{E_{abs}}{E_{ini}} = 1 - \rho_1 + \frac{\rho_1(1-F_{z\to s})(1-\rho)}{1-\rho(1-F)} \tag{24}
$$

The effective albedo of the urban canyon for direct radiation is

$$
\rho_b = 1 - \alpha_b = \rho_1\left[1 - \frac{(1-F_{z\to s})(1-\rho)}{1-\rho(1-F)}\right] \tag{25}
$$

Eq. (25) suggests that the effective albedo of the urban canyon for direct solar radiation depends on wall height, road width, solar position, urban canyon orientation, and the albedo of the canyon surfaces. The albedo of the first reflection ρ_1 is significant to the effective albedo of the urban canyon, and the effective albedo of the urban canyon will not be greater than ρ_1 due to the multiple reflections in the urban canyon.

(2) Multiple reflections of isotropic radiation

Due to the isotropic nature of diffuse solar radiation and downward atmospheric longwave radiation, the albedo of each reflection is ρ. The energy absorbed and reflected after the first reflection is

$$
E_{abs1} = E_{ini}(1-\rho) \tag{26a}
$$

$$
E_{re1} = E_{ini}\rho \tag{26b}
$$

respectively. The reflected energy is divided into the part radiated to the sky, $E_{ini}\rho F$, and the part radiated to the urban canyon, $E_{ini}\rho(1-F)$. The energy absorbed and reflected after the second reflection can be calculated as

$$
E_{abs2} = E_{ini}\rho(1-F)(1-\rho) \tag{27a}
$$

$$
E_{re2} = E_{ini}\rho(1-F)\rho \tag{27b}
$$

The energy absorbed and reflected after *n* reflections can be calculated as

$$
E_{absn} = E_{ini}\rho^{n-1}(1-F)^{n-1}(1-\rho) \tag{28a}
$$

$$
E_{ren} = E_{ini}\rho^{n-1}(1-F)^{n-1}\rho \tag{28b}
$$

The energy absorbed by the urban canyon during all the multiple reflections is

$$
\begin{aligned}
E_{abs} &= E_{abs1} + E_{abs2} + E_{abs3} + \mathrm{L} + E_{absn} \\
&= E_{ini}(1-\rho)(1+\rho(1-F)+\rho^2(1-F)^2 + \mathrm{L} + \rho^n(1-F)^n) \\
&= E_{ini}(1-\rho)\frac{1-\rho^{n+1}(1-F)^{n+1}}{1-\rho(1-F)}
\end{aligned} \tag{29}
$$

In the limit, $n \to \infty$, the energy absorbed after an infinite number of reflections is

$$\lim_{n\to\infty} E_{abs} = E_{ini}\frac{1-\rho}{1-\rho(1-F)} \tag{30}$$

The effective absorptivity of the urban canyon for diffuse and downward atmospheric longwave radiation is

$$\alpha_d = \alpha_l = \frac{1-\rho}{1-\rho(1-F)} \tag{31}$$

The effective albedo of the urban canyon for diffuse, ρ_d, and downward atmospheric longwave radiation, ρ_l, is

$$\rho_d = \rho_l = 1 - \frac{1-\rho}{1-\rho(1-F)} = \frac{\rho F}{1-\rho(1-F)} \tag{32}$$

Eq. (32) suggests that the albedo of the urban canyon for diffuse and downward atmospheric longwave radiation depends on the wall height, road width, and albedo of the urban canyon surfaces. The urban canyon albedo for global solar radiation can be computed by

$$\rho_s = \frac{I_b}{I}\rho_b + \frac{I_d}{I}\rho_d \tag{33}$$

where ρ_s is the urban canyon albedo for global solar radiation, I_b ($\mathrm{W/m^2}$) is direct solar horizontal radiation, I_d ($\mathrm{W/m^2}$) is diffuse solar horizontal radiation, and I ($\mathrm{W/m^2}$) is global solar horizontal radiation. The urban canyon albedo for solar radiation and downward atmospheric longwave radiation is

$$\rho_a = \frac{I_b}{I+I_l}\rho_b + \frac{I_d}{I+I_l}\rho_d + \frac{I_l}{I+I_l}\rho_l \tag{34}$$

where I_l ($\mathrm{W/m^2}$) is downward atmospheric longwave radiation.

2.4 Summary of the model

Two simple formulas, Eq. (25) and Eq. (32), were developed and used to predict the urban canyon albedo for the first time for direct and isotropic radiation. Users can directly calculate UCA without using a complicated process. The UCA of isotropic radiation can be predicted using Eq. (32), which only needs the geometry of the urban canyon and the albedo of its surfaces. If the solar position is obtained, the urban canyon albedo of direct radiation can be calculated according to Eq. (25).

3. Model validation

The model was validated using three scenarios to evaluate its reliability and performance. First, the rationality of the hypothesis of infinite multiple reflections was verified using a typical north-south canyon. Secondly, the analytical results and model outputs under two extreme cases (extreme case 1: very shallow canyon, extreme case 2: bottomless canyon) were compared to verify the robustness of the model. Finally, the model was validated with Aida's experimental test results [51] for an ideal urban canyon and Kotopouleas et al. [50] for an actual urban canyon.

3.1 Validation of multiple reflections

Radiation is reflected in the street canyon until it is entirely absorbed by the surface or escapes from the street canyon. The number of multiple reflections was evaluated until the irradiance emerging from the canyon top or absorbed by urban canyon surfaces fell below a specified threshold value found in previous studies [18,22]. This study assumes that the number of reflections is infinite, $n \to \infty$, and the reliability of this hypothesis was verified by conducting random sampling inspections on different types of canyons. Here the typical north-south urban canyon was analyzed as a case study. The input parameters used in the calculation are shown in Table 1.

Table 1
The input parameters to verify the reliability of infinite multiple reflections.

Input parameters	Values
Solar zenith angle	11.7°
Solar azimuth angle	180°
Direct radiation intensity	500 $\mathrm{W/m^2}$
Canyon orientation	North-south
Road width	5.0 m
Wall height	5.0 m
Albedo of road	0.5
Albedo of walls	0.5

The energy absorbed by the urban canyon after a limited number of multiple reflections is calculated by Eq. (21a), and the energy absorbed by the urban canyon after infinite multiple reflections by Eq. (23). Fig. 5 shows a comparison of results by two calculation methods. All photons are absorbed by the canyon or escape from the canyon top after six reflections, and the energy absorbed by the canyon is 371 $\mathrm{W/m^2}$. The energy absorbed by the canyon after infinite multiple reflections is 372 $\mathrm{W/m^2}$. The energy absorbed by the canyon drops by orders of magnitude after every reflection

inside the canyon, so infinite multiple reflections have no significant effect on the energy absorbed by the canyon. It is therefore simple and effective to set the multiple reflections inside the street canyon to 'n' ($n \to \infty$) times.

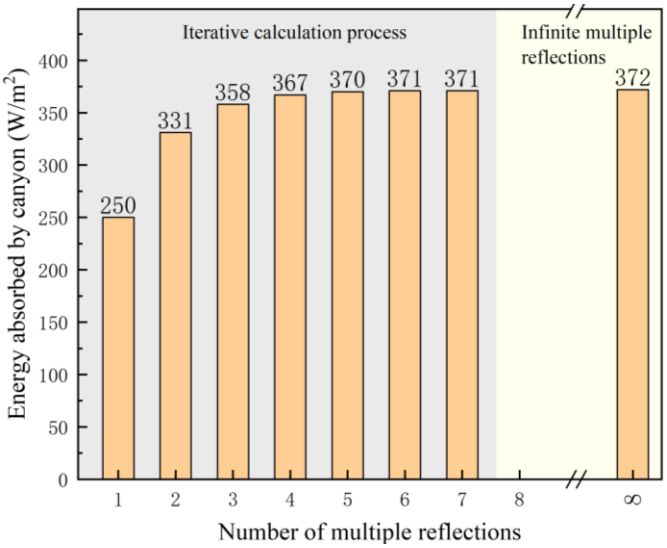

Fig. 5. The number of multiple reflections and the energy absorbed by the canyon.

3.2 Comparing outputs with analytical methods

The model outputs were compared with analytical results under two extreme cases. The input parameters are shown in Table 1. The first extreme case was a very shallow canyon where the canyon aspect ratio was set to 0.01 and 0.001. In this case, the albedo of an urban canyon should be similar to that of a flat surface. The second extreme case was a bottomless canyon where the canyon aspect ratio was set to 100 and 1000. In this case, the urban canyon albedo should approach zero. The model outputs are shown in Table 2. The simulation outputs and the analytical results agree in the two extreme cases. The urban canyon albedo approaches 0.5 when the canyon aspect ratio is smaller than 0.01.

Table 2

Prediction values of the model compared with analytical results.

UCA	Urban canyon aspect ratio			
	0.001	0.01	100	1000
Analytical results	≈0.50	≈0.50	≈0.00	≈0.00
Direct radiation	0.499	0.496	0.005	0.005
Diffuse / longwave radiation	0.499	0.495	0.0005	0.0005

3.3 Comparing outputs with an ideal street canyon experimental test

The model was validated by comparing the simulated outputs with Aida's ideal urban canyon scale model [51]. The scale model was built using a platform of concrete slabs with a diameter of 3m, and various urban structures were created using 0.15m concrete blocks. The experimental albedo tests were conducted in Yokohama, Japan (35°N, 139°E) on June 15 and December 3 using two solar radiometers. Model 1 and model 2 are north-south and east-west oriented canyons with an aspect ratio $h/w = 1.0$ and equal roof and canyon widths as shown in Fig. 6. Many scholars have used this model to validate their urban canyon albedo models [18,22,27,52].

Aida tested the variations in albedo of a uniform flat surface and found that the surface albedo increased near sunrise and sunset due to the dependence of the albedo on the incident angle of the surfaces. The albedo of the roof was set as the albedo measured from the flat surface by Aida [51], and the albedos of the wall and road are taken as a constant, equal to 0.414 according to the literature [24]. The diffuse and total solar radiation ratio was set to 0.177 to represent a typical sunny day because the experiment data was measured on clear days.

The root mean square error (*RMSE*) and Pearson correlation coefficient (*r*) were used to evaluate the model's predicted performance. They are calculated as follows:

$$RMSE = \sqrt{\frac{\sum_{i=1}^{n}(P_i - M_i)^2}{n}} \tag{35}$$

$$r = \frac{\sum_{i=1}^{n}(P_i - \bar{P})(M_i - \bar{M})}{\sqrt{\sum_{i=1}^{n}(P_i - \bar{P})^2}\sqrt{\sum_{i=1}^{n}(M_i - \bar{M})^2}} \tag{36}$$

where P_i is the *i*th predicted value, M_i is the *i*th measured value, and *n* is the number for comparison. $\bar{P}$ is the average of the predicted value, and $\bar{M}$ is the average of the measured value.

A comparison of predicted and measured values during the summer is shown in Fig. 6a. Overall, the simulated values are slightly larger than the measured values. Slight deviations are also found when the albedo measured in the winter is validated (Fig. 6b). Possible reasons for these deviations are uncertainties associated with the local atmospheric conditions and possible observation errors. We compared the prediction performance of the new model to three existing models, as shown in Table 3. The new model has a Pearson correlation coefficient of 0.87 for summer and 0.95 for winter. The maximum *RMSE* is less than 0.018. Despite the simplicity of the calculation method, the new model guarantees calculation accuracy compared with other models.

Table 3

The prediction performance of the model compared with other models.

Model type	Present model		Sailor's model [18]		Fortuniak's model [27]		Qin's model [22]	
	Summer	Winter	Summer	Winter	Summer	Winter	Summer	Winter
RMSE	0.018	0.016	0.019	0.022	0.011	0.022	0.018	0.021
r	0.87	0.95	0.74	0.89	0.92	0.96	0.82	0.96

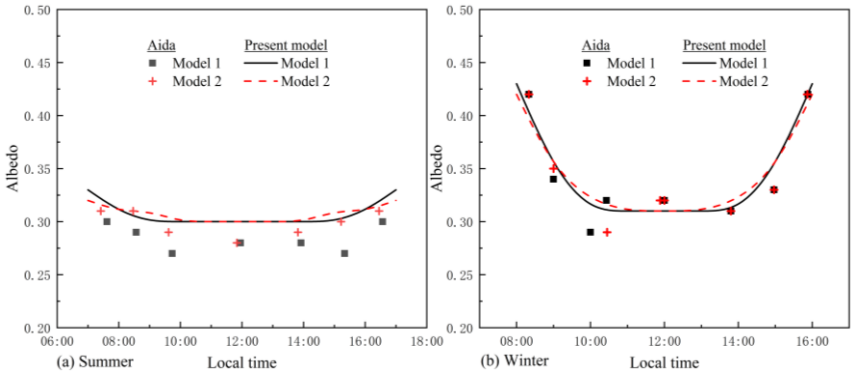

Fig. 6. Validation results comparing present model outputs to ideal experimental data for measurements in (a) June and (b) December. Note: Model 1 is a north-south orientation urban canyon; Model 2 is an east-west orientation urban canyon; dotted data is the measured data digitized from Aida [51]; the solid line represents the output from the model.

3.4 Comparing outputs with an actual street canyon experimental test

The model was validated by comparing the results with a complex street canyon experimental test by Kotopouleas *et al*. [50] who developed a scale model of an actual residential area in Islington, London. The northeast-southwest oriented street canyon consists of 22 trapezoidal, 3-story building blocks with an aspect ratio of 1/1.6. The diurnal UCAs of three facade types: Brickwork (73% bricks, 24% glass, and 3% wood); Curtain Wall (3m^2 on each side covering 40-44% of the facade); and Aluminium cladding (3m^2 on each side covering 40-44% of the facade) were used to validate our model. The ground status was 82% tarmac and 18% paving. According to their material library, we calculated the mean albedo of facades and ground as inputs to the model. The mean albedo for brickwork, curtain wall, aluminum cladding, and ground is 0.25, 0.17, 0.23, and 0.14, respectively.

The results (Fig. 7) revealed a good convergence between the model outputs and measured values. The UCA of all facade types presented a U-shaped profile due to pavement surface albedo being high at sunrise and sunset and low and constant over

midday [53]. The UCA in the morning and evening was not simulated due to the lack of surface albedo. However, the estimated values for the daytime show that the model has a reasonable degree of accuracy. Compared with measurement results, the Pearson correlation coefficient for brickwork, curtain wall, and aluminum cladding is 0.75, 0.63, and 0.74, respectively, and the *RMSE* is 0.016, 0.03, and 0.012, respectively. The validation results show that the model can simulate the UCA of complex street canyons when reasonable boundary conditions are given.

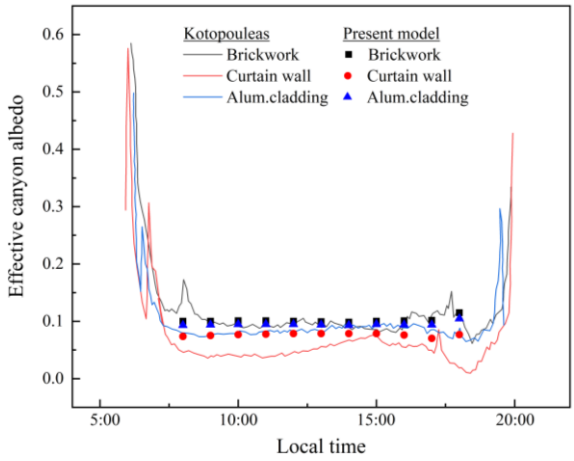

Fig. 7. Validation results comparing present model outputs to complex experimental data. Note: the solid lines are the measured data digitized from Kotopouleas [50], while the dotted data represents the output from the model.

4. Model Applications

This section demonstrates the application of the newly developed model. First, this model can be used to calculate the UCA of a given street canyon and evaluate the effect of the urban geometry and materials on the UCA. Secondly, quickly estimating the solar performance at the urban scale is another contribution of this model.

4.1 UCA estimation of an urban canyon and sensitivity analysis

The diurnal variations and influencing factors of UCA on a typical summer day were analyzed, taking Chongqing (30°N, 126°E) in China as a case study. The weather data on July 27 of a typical meteorological year for Chongqing was used in this simulation [54]. The UCA of downward atmospheric longwave radiation is not analyzed because it is the same as diffuse solar radiation. The albedo of roofs on both sides of the street canyon is no longer considered to show UCA variations separately.

4.1.1 UCA variations with aspect ratio and canyon orientation

The urban canyon geometry controls the UCA. Street canyon aspect ratio and orientation are the most important parameters reflecting street canyon geometry [55,56]. The urban canyon aspect ratio was set to 0.1, 0.3, 0.5, 0.75, 1.0, 3.0, 5.0, 7.5, and 10.0 to represent an urban canyon with different depths. The albedo of both the road and walls was set to 0.5 to observe more obvious albedo variations.

First, the UCA hourly variations of the direct, diffuse, and global solar radiation of north-south (N-S) and east-west (E-W) orientation urban canyons with different aspect ratios were investigated (Fig. 8). The UCA of direct solar radiation varies slightly from 6:00 to 18:00 (Fig. 8a) in the N-S canyon when the canyon is shallow ($h/w < 1$). Usually, there is a large UCA at noon; this has an opposite trend to the measurement results of Aida because this model did not capture the dependence of surface albedo on the incidence angle, which is a common defect of that urban canyon radiation model [18,22,27]. The simulation results are smaller than the actual situation at sunrise and sunset. The diurnal UCA variation trends of direct solar radiation in the E-W canyon (Fig. 8b) are similar to the N-S canyon when the canyon is shallow, possibly because the variations of $F_{z\to s}$ are slight due to lower walls. The UCA variation trends in direct solar radiation predicted in this paper agree with those by Qin [22].

The UCA of direct solar radiation in the N-S canyon follows a V-shape when the aspect ratio is larger than 3.0, as shown in Fig. 8a. Only the upper part of the wall is illuminated due to the large solar zenith angle at sunrise and sunset and the amount of solar radiation escaping directly out of the street canyon. The multiple reflections and absorption of direct solar radiation inside the canyon severely reduced the UCA during the daytime. The UCA of direct solar radiation has a minimum value at noon and then increases gradually with the increase in the solar zenith angle.

The direct solar radiation in the E-W canyon follows a W-shape when the aspect ratio is larger than 3.0, as shown in Fig. 8b. The maximum UCA of direct solar radiation occurs at sunrise before dropping sharply and reaching its lowest value at 8:00 and then increasing slightly. The second trough occurs at 16:00 local time. This phenomenon is related to the shadow length, which is discussed in the latter part of this section. The variation trends of direct solar radiation predicted in this paper agree with those by Fortuniak [27].

The UCA of diffuse solar radiation remains constant due to its isotropic nature. The UCA of diffuse solar radiation decreases with an increased canyon aspect ratio and

is not affected by the canyon orientation. The UCA for diffuse solar radiation in the N-S canyon (Fig. 8c) and E-W canyon (Fig. 8d) is the same, as can also be verified by Eq. (32). Due to diffuse solar radiation accounting for only a tiny part of global solar radiation, the UCA of global solar radiation (Fig. 8e, Fig. 8f) is the same as direct solar radiation.

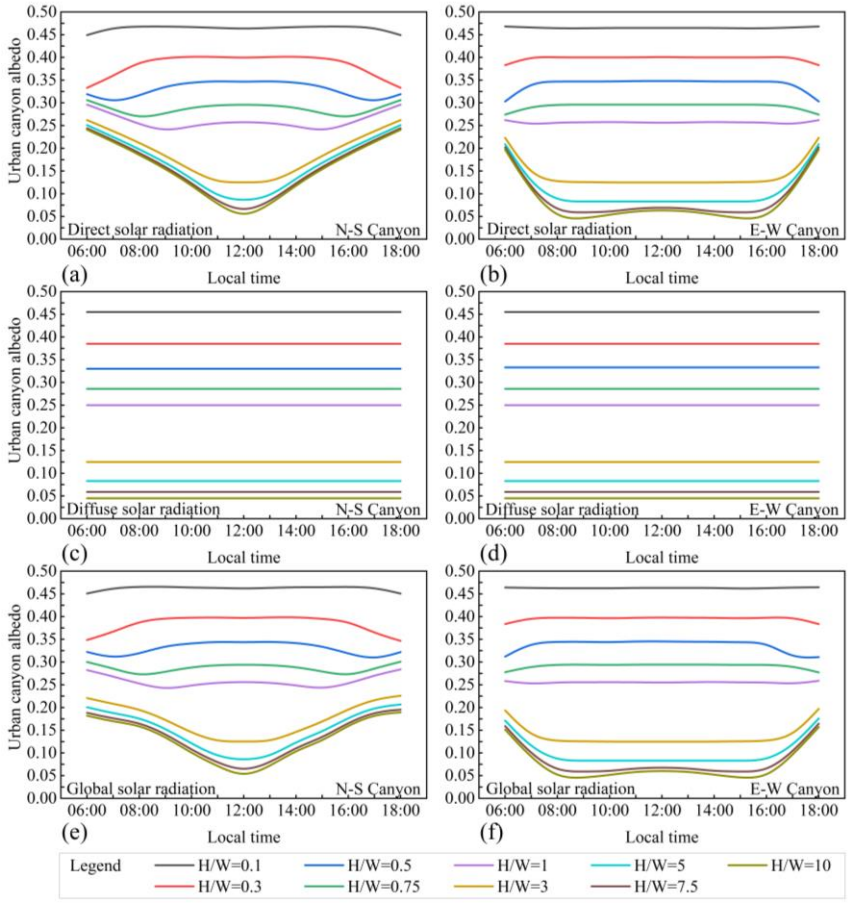

Fig. 8. Diurnal variations of UCA on July 27 in Chongqing.

Fig. 9 illustrates the relationship between the daily mean UCA and urban canyon aspect ratio in different orientations. The canyon aspect ratio significantly influences the UCA of direct solar radiation. UCA decreases sharply with an increase in the canyon aspect ratio when the canyon ratio is less than 1.0 (Fig. 9a), and different orientations of canyons have the same variation trends. The UCA of direct solar radiation in a N-S canyon is 0.47, 0.34, and 0.25 for a canyon aspect ratio of 0.1, 0.5, and 1.0, respectively.

The UCA of direct solar radiation changes gradually with the canyon aspect ratio when the canyon aspect ratio increases and the UCA begins to vary with canyon orientation. The UCA of direct solar radiation for a N-S canyon and an E-W canyon are 0.16 and 0.13, respectively, when the canyon aspect ratio is 3.0. When the canyon aspect ratio is greater than 4.0, increasing the canyon aspect ratio affects the UCA slightly. The UCA of direct solar radiation in the N-S canyon is 0.14, 0.13, and 0.12 for a canyon aspect ratio of 5.0, 7.5, and 10, respectively. The E-W canyon has a lower UCA than canyons in any other direction.

Fig. 9b shows that the UCA of diffuse solar radiation decreases with increasing canyon aspect ratio. This influence gradually weakens with a canyon aspect ratio greater than 4.0, similar to the observations made for direct solar radiation. The canyon orientation does not affect the UCA of diffuse solar radiation, so there is only one curve in Fig. 9b. The variations of UCA of global solar radiation are the same as direct solar radiation, as shown in Fig. 9c.

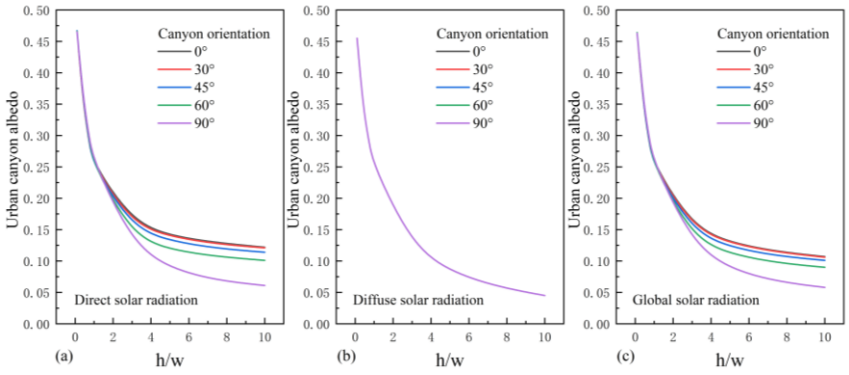

Fig. 9. Relationship between the urban canyon albedo and the canyon aspect ratio.

The influence of canyon orientation on the average daily UCA was calculated. Fig. 10a shows that the canyon orientation slightly affects UCA when the canyon aspect ratio is less than 1.0. The UCA gradually decreases as the canyon azimuth angle increases. The UCA of the N-S canyon is 0.16, 0.14, 0.13, and 0.12 for an aspect ratio of 3.0, 5.0, 7.5, and 10.0, respectively whilst the UCA of the E-W canyon is 0.13, 0.09, 0.07, and 0.06 for an aspect ratio of 3.0, 5.0, 7.5, and 10.0, respectively. Usually, the N-S canyon has the maximum UCA, and the E-W canyon has the minimum UCA. Because the N-S canyon will produce shadows for a longer period during the day for a deep urban canyon, that is to say, direct solar radiation mainly illuminates the canyon walls,

and the radiation can escape from the canyon top more easily. The canyon orientation does not affect the UCA of diffuse solar radiation, as shown in Fig. 10b. The variations of UCA of global solar radiation with canyon orientation are the same as for direct solar radiation, as shown in Fig. 10c.

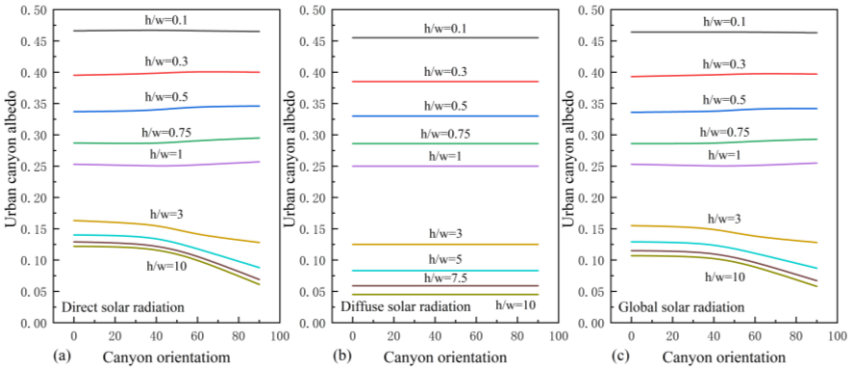

Fig. 10. Relationship between the urban canyon albedo and the canyon orientation.

The distribution of direct solar radiation in a deep urban canyon was analyzed, taking an urban canyon with a road width of 1m and a wall height of 5m, as shown in Fig. 11. For the N-S canyon, a small part of the north wall is sunlit at sunrise, and the sunlit area gradually increases as the solar zenith angle decreases. The road inside the canyon is sunlit at 11:15 and is fully sunlit at noon, and the UCA of direct solar radiation has the minimum value in this period. The period that the road is sunlit is no more than 2 hours. For the E-W canyon, the road inside the canyon is sunlit at around 7:45, and the period for which the road is sunlit is about 8 hours, which results in more multiple reflections and more solar radiation being absorbed by the urban canyon. The direct radiation distribution of canyons with different orientations was also reported by Lau *et al*. [57] and Ali-Toudert *et al*. [58].

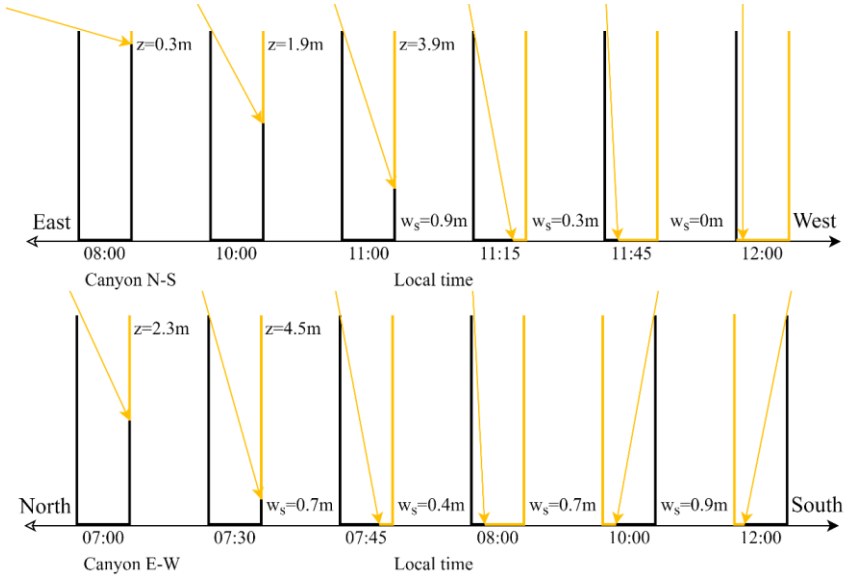

Fig. 11. Direct solar radiation distribution in a deep urban street canyon.

In summary, canyon orientation slightly affects UCA for shallow canyons. For deep canyons, N-S and E-W canyons have the maximum and minimum UCA, respectively, because, as the azimuth angle of the canyon increases, the exposure period of the road gradually increases.

4.1.2 UCA variations with albedos of pavements and walls

Portland cement concrete and asphalt are the most commonly used pavement materials in today's urban environment. Generally, the albedo of new conventional grey Portland cement concrete is 0.35-0.40, and aged Portland cement concrete has an albedo of 0.20-0.30 [59]. The albedo of new asphalt is very low, the surface becomes lighter after long-term use, and the albedo of aged asphalt is about 0.2 [60]. High albedo pavements have always been used as one of the main methods of improving the urban thermal environment and have been extensively studied [61–63]. This study simulated an UCA with a fixed wall albedo of 0.3 but with different road albedo values (0.2, 0.3 for a regular pavement; 0.4, 0.5, and 0.6 for a high albedo pavement). Only the N-S canyon was analyzed. The aspect ratio was set to 0.1, 0.5, 1.0, 5.0, and 10.0 to represent canyons with different depths.

Fig. 12 shows the variations in UCA for different pavement albedo values, an increase in pavement albedo can significantly increase the UCA for shallow urban

canyons ($h/w \leq 1.0$). As the aspect ratio increases, the effect of pavement albedo on UCA gradually weakens. Road albedo has little impact on the UCA when the aspect ratio of the canyon is greater than 1.0, as shown in Fig. 12a. Because the road is only exposed to sunlight for a short time, the multiple reflections severely reduce the UCA for the deep canyon. Therefore, the UCA of direct radiation can be effectively reduced by increasing the road albedo for shallow canyons ($h/w \leq 1.0$), but the high albedo pavement has little effect on the UCA of direct radiation for deep canyons.

The variation trends of UCA for diffuse solar radiation are the same as for direct solar radiation, as shown in Fig. 12b. The UCA of diffuse solar radiation is mainly affected by the wall albedo because the proportional contribution of the road is negligible for deep canyons. Hence, high albedo pavements can reduce the solar energy absorbed by canyons for shallow canyons, but this method becomes less effective for deep canyons.

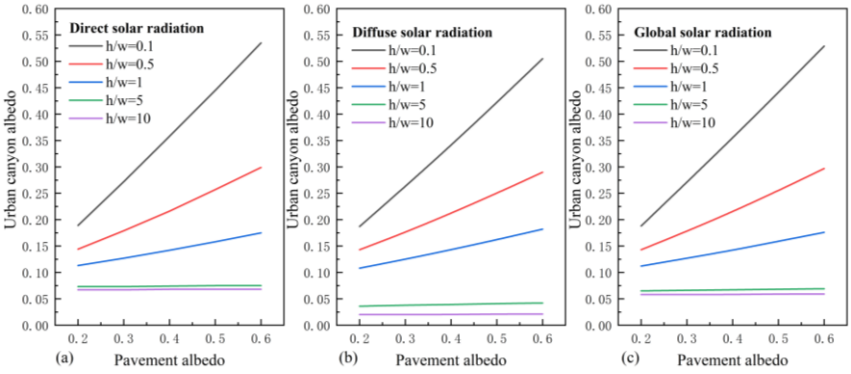

Fig. 12. The influence of the pavement albedo on the urban canyon albedo.

The effect of wall albedo on the UCA was also analyzed. This study simulated the UCA with a fixed road albedo of 0.3 but with different wall albedo values (0.2, 0.3, 0.4, 0.5, and 0.6). The aspect ratio was set to 0.1, 0.5, 1.0, 5.0, and 10.0 to represent canyons with different depths.

Fig. 13a indicates that high albedo walls effectively increase the UCA of direct solar radiation for shallow and deep urban canyons. Wall albedo rises from 0.2 to 0.6 resulting in an increase in UCA of direct solar radiation from 0.26 to 0.3 for a shallow urban canyon with an aspect ratio of 0.1, as shown in Table 4. For a deep urban canyon with an aspect ratio of 10.0, increasing wall albedo to 0.6 leads to an increase of 0.16 in UCA for direct solar radiation. Increasing the albedo of walls can raise the UCA of

direct solar radiation more effectively than the road albedo since the walls are usually exposed to direct solar radiation for longer periods, even in deep canyons.

Table 4

UCA of direct solar radiation with different wall albedo and aspect ratio values.

Wall albedo	Urban canyon aspect ratio				
	0.1	0.5	1.0	5.0	10.0
0.2	0.26	0.15	0.09	0.05	0.04
0.6	0.30	0.29	0.26	0.18	0.16

High albedo walls can effectively increase the UCA for shallow and deep canyons for diffuse solar radiation, as shown in Fig. 13b. It is worth noting that although the UCA variation trends of diffuse solar radiation and direct solar radiation with wall albedo are consistent, the influence mechanism is different. The variations of diffuse solar radiation are not affected by solar position. All methods to increase the average albedo of the surface inside the canyon can effectively increase the UCA of diffuse solar radiation. Compared with roads, increasing wall albedo can effectively improve the UCA of diffuse solar radiation because the walls account for a relatively large proportion, even in deeper urban canyons. The variations of UCA of global solar radiation are the same as for direct solar radiation due to the large proportion of direct solar radiation, as shown in Fig. 13c.

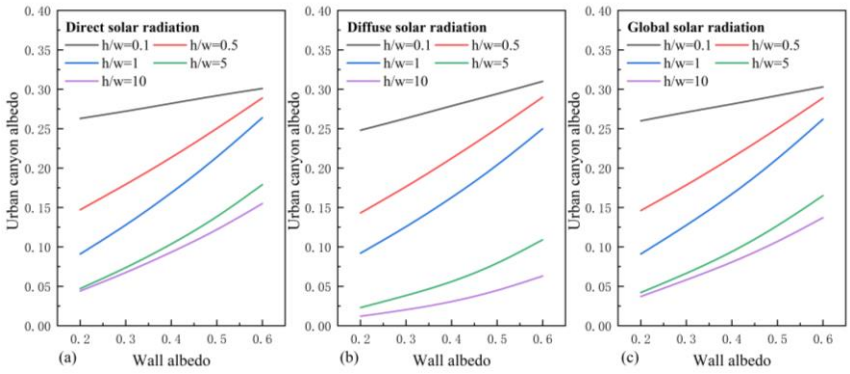

Fig. 13. The influence of the wall albedo on the urban canyon albedo.

4.2 Urban-scale solar performance estimation

The newly-developed model can rapidly assess street canyon radiation at urban scales. The model is used to calculate the solar radiation absorbed by the street canyons with 300m resolution at the urban scale - taking London (51°N, 0°E) as an example in this section. Meteorological data for a typical summer day (June 21, 2018) are selected

in this simulation. Surface classification (25m resolution) and digital elevation model (DEM) (1m resolution) data for the entire London area were utilized for the case study illustration, which was produced by UKCEN [64]. Firstly, DEM was used to extract the urban geometry parameters (average wall albedo, average pavement albedo, canyon orientation, and aspect ratio of the street canyon) through raster data spatial analysis methods in the geographic information system (GIS). And then, the average UCA and solar radiation absorbed by the urban canyon were estimated using our model. The entire process was completed within 1 hour, providing a new method to quickly estimate urban-scale solar radiation performance.

The specific operation process is as follows. First, the land cover classification and DEM data (Fig. 14) were reclassified to set the surface albedo and wall albedo parameters. The ground cover was divided into six categories: buildings, pavement, trees, grass, bare soil, and water. According to the height, the classification of walls is simply divided into three different facades (less than 10m, 10m to 30m, and above 30m). Secondly, the determination of the street orientation is obtained by indirectly judging the direction of the building walls and then converting them. Specifically, the orientation of the building wall can be obtained by performing gradient analysis on the DEM data (that is, judging the direction in which the elevation changes).

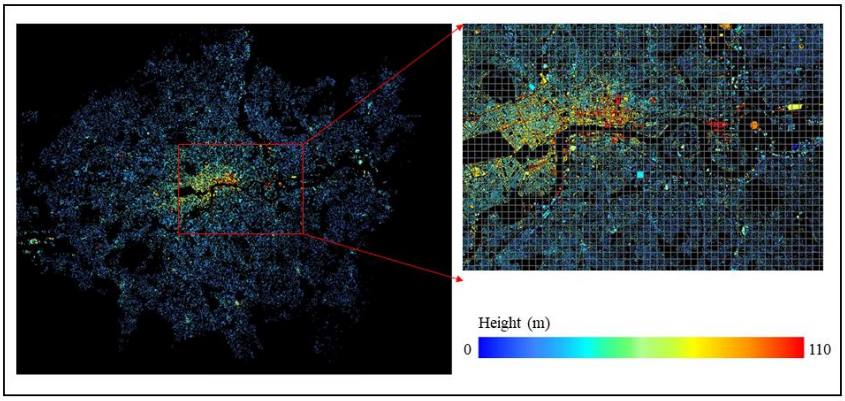

Fig. 14. The DEM data for London.

Since the wall orientation is always perpendicular to the street orientation, the street orientation can be obtained by converting the calculated wall orientation by 90 degrees. Third, similar to getting the direction of the wall, the boundary of the building (that is, the position where the gradient value changes the most) can be judged by the

gradient calculation. When the building boundary is obtained, the numerical surface area of the building can be calculated by combining its elevation information. Then, the canyon aspect ratio can be obtained by comparing the calculated vertical surface area with the street area in the DEM with the value of 0. Finally, with the help of the zonal statistical calculation method of raster data, all the above parameters are statistically calculated for all of London according to each 300m*300m grid to obtain the average value. The average DEM data with 300m resolution is shown in Fig. 15. The averaged DEM data is in good agreement with the original data (Fig. 14).

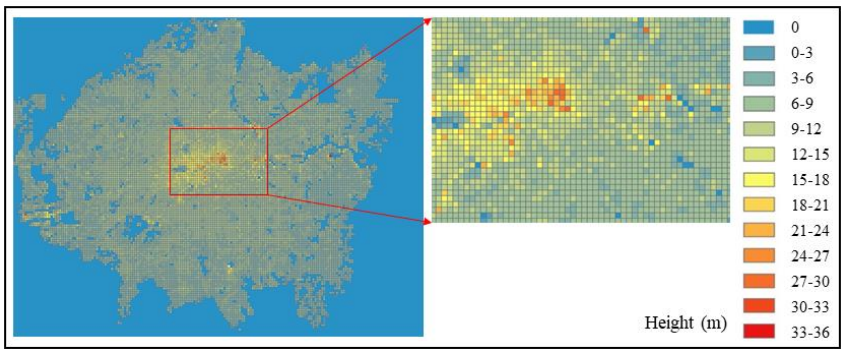

Fig. 15. The average DEM data of London at 300m resolution.

The hourly solar radiation absorbed by street canyons in London was calculated using the model developed in this study. Fig. 16 shows the absorbed solar radiation at noon. As a whole, the solar radiation absorbed by urban canyons in London is radial, the solar radiation absorbed by the central urban area is significantly higher than that of the surrounding areas. The variation trend of solar radiation absorption is the same as the variation trend of building height, which shows that the aspect ratio of street canyons plays a decisive role in the amount of solar radiation absorbed by street canyons.

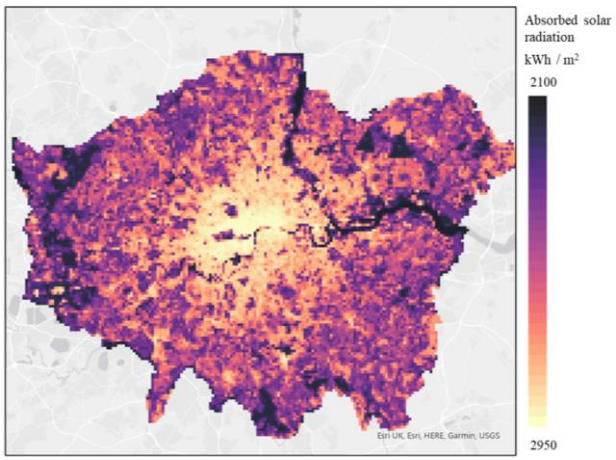

Fig. 16. Solar radiation absorbed by street canyons in London at noon on June 21, 2018.

Fig. 17 shows the daily variation of solar radiation absorbed by street canyons in London. The amount of solar radiation absorbed by urban street canyons has an evident daily variation. The maximum solar radiation absorption at noon is about 3000 kWh/m^2, and the radiation absorption at 18:00 local time is only about one-fourth of the solar radiation absorption at noon. Our simulation results are consistent with the trends in surface temperature and heat island intensity distribution in London [65], suggesting that combining our model with DEM data is an efficient way to rapidly estimate the radiation performance of a large-scale urban canyon.

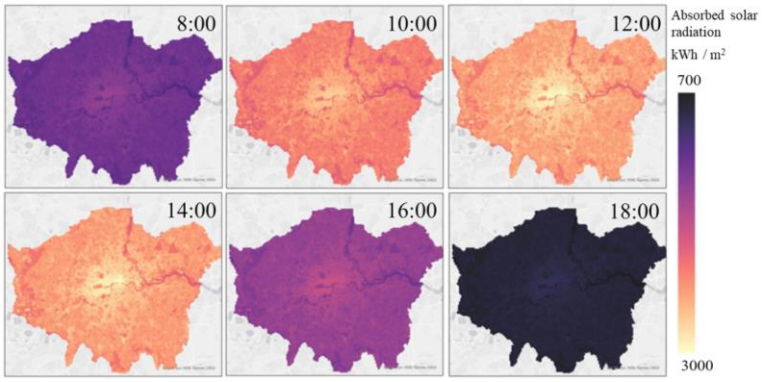

Fig. 27. The daily variation of solar radiation absorbed by street canyons in London on June 21, 2018.

5 Model limitations

The model uses the assumptions and simplifications commonly used in the urban canyon model. Firstly, all surface elements of the urban canyon are Lambertian, but the reflectivity of many actual structures depends on the incident angle. Secondly, the other objects in the street are neglected, especially trees. With the development of green cities, trees have become a ubiquitous and non-negligible part of the cityscape and have changed the radiation transmission path in street canyons. This limitation will be considered in a future model. Even if the above assumptions affect the accuracy of the model, the model provides a robust theoretical calculation for quickly assessing the urban canyon radiation performance.

6 Conclusions

This paper presents a newly-developed simplistic but robust mathematical model for a rapid calculation of urban canyon albedo (UCA). The model can effectively predict the UCA with various canyon geometries and building surface construction materials in any location. The model has been validated with experimental tests, the maximum root mean square error (*RMSE*) is 0.03, and the minimum Pearson correlation coefficient (*r*) is 0.63.

The diurnal variations and influencing factors of UCA on a typical summer day were analyzed using a case study in Chongqing, China. It was found that the canyon aspect ratio determines the UCA, especially when the canyon aspect ratio is less than 4. The canyon orientation has almost no effect on UCA when the canyon aspect ratio is less than 1. High albedo pavements can effectively increase the UCA when the canyon aspect ratio is less than 1. The building wall albedo has a higher impact on UCA than the one of the pavement.

The newly developed UCA calculation algorithm integrated with urban building information in the GIS platform can rapidly calculate city-scale UCA. The implementation of the model for the City of London has been demonstrated. The model can be used to assess the impacts of urban geometry and materials on radiation performance on the block and urban scale quickly.

Acknowledgments

The research is supported by the Fundamental Research Funds for the Central Universities, China [Grant No. 2021CDJCGJ015] and the Natural Science Foundation

of Chongqing, China [Grant No. cstc2021ycjh-bgzxm0156].

References

[1] M. Santamouris, C. Cartalis, A. Synnefa, D. Kolokotsa, On the impact of urban heat island and global warming on the power demand and electricity consumption of buildings—A review, Energy and Buildings. 98 (2015) 119–124. https://doi.org/10.1016/j.enbuild.2014.09.052.

[2] L. Xu, J. Wang, F. Xiao, S. EI-Badawy, A. Awed, Potential strategies to mitigate the heat island impacts of highway pavement on megacities with considerations of energy uses, Applied Energy. 281 (2021) 116077. https://doi.org/10.1016/j.apenergy.2020.116077.

[3] E. Jamei, P. Rajagopalan, M. Seyedmahmoudian, Y. Jamei, Review on the impact of urban geometry and pedestrian level greening on outdoor thermal comfort, Renewable and Sustainable Energy Reviews. 54 (2016) 1002–1017. https://doi.org/10.1016/j.rser.2015.10.104.

[4] C. Mora, B. Dousset, I.R. Caldwell, F.E. Powell, R.C. Geronimo, C.R. Bielecki, C.W.W. Counsell, B.S. Dietrich, E.T. Johnston, L.V. Louis, M.P. Lucas, M.M. McKenzie, A.G. Shea, H. Tseng, T.W. Giambelluca, L.R. Leon, E. Hawkins, C. Trauernicht, Global risk of deadly heat, Nature Climate Change. 7 (2017) 501–506. https://doi.org/10.1038/nclimate3322.

[5] D. Lai, W. Liu, T. Gan, K. Liu, Q. Chen, A review of mitigating strategies to improve the thermal environment and thermal comfort in urban outdoor spaces, Science of The Total Environment. 661 (2019) 337–353. https://doi.org/10.1016/j.scitotenv.2019.01.062.

[6] Y. Li, S. Schubert, J.P. Kropp, D. Rybski, On the influence of density and morphology on the Urban Heat Island intensity, Nature Communications. 11 (2020) 1–9.

[7] B.-J. He, L. Ding, D. Prasad, Relationships among local-scale urban morphology, urban ventilation, urban heat island and outdoor thermal comfort under sea breeze influence, Sustainable Cities and Society. 60 (2020) 102289. https://doi.org/10.1016/j.scs.2020.102289.

[8] P. Coseo, L. Larsen, Cooling the Heat Island in Compact Urban Environments: The Effectiveness of Chicago's Green Alley Program, Procedia Engineering. 118 (2015) 691–710. https://doi.org/10.1016/j.proeng.2015.08.504.

[9] J. Yang, Z.-H. Wang, K.E. Kaloush, H. Dylla, Effect of pavement thermal properties on mitigating urban heat islands: A multi-scale modeling case study in Phoenix, Building and Environment. 108 (2016) 110–121. https://doi.org/10.1016/j.buildenv.2016.08.021.

[10] J. Wei, J. He, Numerical simulation for analyzing the thermal improving effect of evaporative cooling urban surfaces on the urban built environment, Applied Thermal Engineering. 51 (2013) 144–154. https://doi.org/10.1016/j.applthermaleng.2012.08.064.

741 [11] M. Santamouris, F. Fiorito, On the impact of modified urban albedo on ambient
742 temperature and heat related mortality, Solar Energy. 216 (2021) 493–507.
743 https://doi.org/10.1016/j.solener.2021.01.031.
744 [12] A. Mohammed, A. Khan, M. Santamouris, On the mitigation potential and
745 climatic impact of modified urban albedo on a subtropical desert city, Building
746 and Environment. 206 (2021) 108276.
747 https://doi.org/10.1016/j.buildenv.2021.108276.
748 [13] D. Groleau, P.G. Mestayer, Urban Morphology Influence on Urban Albedo: A
749 Revisit with the Solene Model, Boundary-Layer Meteorol. 147 (2013) 301–327.
750 https://doi.org/10.1007/s10546-012-9786-6.
751 [14] S. Godinho, A. Gil, N. Guiomar, M.J. Costa, N. Neves, Assessing the role of
752 Mediterranean evergreen oaks canopy cover in land surface albedo and
753 temperature using a remote sensing-based approach, Applied Geography. 74
754 (2016) 84–94. https://doi.org/10.1016/j.apgeog.2016.07.004.
755 [15] F. Despini, C. Ferrari, G. Santunione, S. Tommasone, A. Muscio, S. Teggi, Urban
756 surfaces analysis with remote sensing data for the evaluation of UHI mitigation
757 scenarios, Urban Climate. 35 (2021) 100761.
758 https://doi.org/10.1016/j.uclim.2020.100761.
759 [16] G.A. Ban-Weiss, J. Woods, R. Levinson, Using remote sensing to quantify albedo
760 of roofs in seven California cities, Part 1: Methods, Solar Energy. 115 (2015) 777–
761 790. https://doi.org/10.1016/j.solener.2014.10.022.
762 [17] M.V.B. de Morais, E.R. Marciotto, V.V. Urbina Guerrero, E.D. de Freitas,
763 Effective albedo estimates for the Metropolitan Area of São Paulo using empirical
764 sky-view factors, Urban Climate. 21 (2017) 183–194.
765 https://doi.org/10.1016/j.uclim.2017.06.007.
766 [18] D.J. Sailor, H. Fan, Modeling the diurnal variability of effective albedo for cities,
767 Atmospheric Environment. 36 (2002) 713–725. https://doi.org/10.1016/S1352-
768 2310(01)00452-6.
769 [19] F. Ali-Toudert, Exploration of the thermal behaviour and energy balance of urban
770 canyons in relation to their geometrical and constructive properties, Building and
771 Environment. 188 (2021) 107466.
772 https://doi.org/10.1016/j.buildenv.2020.107466.
773 [20] S. Cohen, Y. Palatchi, D.P. Palatchi, L. Shashua-Bar, V. Lukyanov, Y. Yaakov, A.
774 Matzarakis, J. Tanny, O. Potchter, Mean radiant temperature in urban canyons
775 from solar calculations, climate and surface properties – Theory, validation and
776 'Mr.T' software, Building and Environment. 178 (2020) 106927.
777 https://doi.org/10.1016/j.buildenv.2020.106927.
778 [21] E. Andreou, The effect of urban layout, street geometry and orientation on shading
779 conditions in urban canyons in the Mediterranean, Renewable Energy. 63 (2014)
780 587–596. https://doi.org/10.1016/j.renene.2013.09.051.
781 [22] Y. Qin, Urban canyon albedo and its implication on the use of reflective cool
782 pavements, Energy and Buildings. 96 (2015) 86–94.

783 https://doi.org/10.1016/j.enbuild.2015.03.005.
784 [23] National Bureau of Statistics. http://www.stats.gov.cn/ (accessed April 21, 2021)
785 (in Chinese).
786 [24] M. Aida, K. Gotoh, Urban albedo as a function of the urban structure — A two-
787 dimensional numerical simulation, Boundary-Layer Meteorol. 23 (1982) 415–424.
788 https://doi.org/10.1007/BF00116270.
789 [25] A.J. Arnfield, An approach to the estimation of the surface radiative properties and
790 radiation budgets of cities, Physical Geography. 3 (1982) 97–122.
791 https://doi.org/10.1080/02723646.1982.10642221.
792 [26] Y. Sakakibara, A numerical study of the effect of urban geometry upon the surface
793 energy budget, Atmospheric Environment. 30 (1996) 487–496.
794 https://doi.org/10.1016/1352-2310(94)00150-2.
795 [27] K. Fortuniak, Numerical estimation of the effective albedo of an urban canyon,
796 Theoretical and Applied Climatology. 91 (2008) 245–258.
797 https://doi.org/10.1007/s00704-007-0312-6.
798 [28] L. Qing, W. Yunlong, F. Xiaokai, W. Hanbin, A.-H. Sulala, Solution of integrated
799 reflection for cities, Journal of civil and environmental engineering. 37 (2015) 7-
800 11+17 (in Chinese).
801 [29] M.J.N.O. Panão, H.J.P. Gonçalves, P.M.C. Ferrão, A Matrix Approach Coupled
802 with Monte Carlo Techniques for Solving the Net Radiative Balance of the Urban
803 Block, Boundary-Layer Meteorol. 122 (2007) 217–241.
804 https://doi.org/10.1007/s10546-006-9088-y.
805 [30] X. Yang, Y. Li, The impact of building density and building height heterogeneity
806 on average urban albedo and street surface temperature, Building and
807 Environment. 90 (2015) 146–156. https://doi.org/10.1016/j.buildenv.2015.03.037.
808 [31] E.S. Krayenhoff, A. Christen, A. Martilli, T.R. Oke, A Multi-layer Radiation
809 Model for Urban Neighbourhoods with Trees, Boundary-Layer Meteorology. 151
810 (2014) 139–178. https://doi.org/10.1007/s10546-013-9883-1.
811 [32] J.P. Montávez, J.I. Jiménez, A. Sarsa, A Monte Carlo Model Of The Nocturnal
812 Surface Temperatures In Urban Canyons, Boundary-Layer Meteorology. 96 (2000)
813 433–452. https://doi.org/10.1023/A:1002600523841.
814 [33] X. He, H. Yu, J. Li, L. Ding, The solving formula of the solar azimuth angle and
815 its applications, Acta Energiae Solaris Sinica. 29 (2008) 69–73 (in Chinese).
816 [34] J. Tang, Y. Wang, D. Zhao, X. Guo, J. Zhao, C. Shen, J. Liu, Application of
817 polarized light compass system on solar position calculation, Optik. 187 (2019)
818 135–147. https://doi.org/10.1016/j.ijleo.2019.04.129.
819 [35] M. Blanco-Muriel, D.C. Alarcón-Padilla, T. López-Moratalla, M. Lara-Coira,
820 Computing the solar vector, Solar Energy. 70 (2001) 431–441.
821 https://doi.org/10.1016/S0038-092X(00)00156-0.
822 [36] I. Reda, A. Andreas, Solar position algorithm for solar radiation applications, Solar
823 Energy. 76 (2004) 577–589. https://doi.org/10.1016/j.solener.2003.12.003.
824 [37] R. Grena, An algorithm for the computation of the solar position, Solar Energy. 82

(2008) 462–470. https://doi.org/10.1016/j.solener.2007.10.001.
[38] J. Boland, L. Scott, M. Luther, Modelling the diffuse fraction of global solar radiation on a horizontal surface, Environmetrics. 12 (2001) 103–116. https://doi.org/10.1002/1099-095X(200103)12:2<103::AID-ENV447>3.0.CO;2-2.
[39] S. Ener Rusen, A. Konuralp, Quality control of diffuse solar radiation component with satellite-based estimation methods, Renewable Energy. 145 (2020) 1772–1779. https://doi.org/10.1016/j.renene.2019.07.085.
[40] J.C. Lam, D.H.W. Li, Correlation between global solar radiation and its direct and diffuse components, Building and Environment. 31 (1996) 527–535. https://doi.org/10.1016/0360-1323(96)00026-1.
[41] L. Benali, G. Notton, A. Fouilloy, C. Voyant, R. Dizene, Solar radiation forecasting using artificial neural network and random forest methods: Application to normal beam, horizontal diffuse and global components, Renewable Energy. 132 (2019) 871–884. https://doi.org/10.1016/j.renene.2018.08.044.
[42] J.F. Orgill, K.G.T. Hollands, Correlation equation for hourly diffuse radiation on a horizontal surface, Solar Energy. 19 (1977) 357–359. https://doi.org/10.1016/0038-092X(77)90006-8.
[43] C. Rensheng, K. Ersi, Y. Jianping, L. Shihua, Z. Wenzhi, D. Yongjian, Estimation of horizontal diffuse solar radiation with measured daily data in China, Renewable Energy. 29 (2004) 717–726. https://doi.org/10.1016/j.renene.2003.09.012.
[44] S.A. Kalogirou, Solar Energy Engineering: Processes and Systems, Academic Press, 2013.
[45] ASTM, Standard Solar Constant and Zero Air Mass Solar Spectral Irradiance Tables, American Society for Testing and Materials, 2019. http://www.astm.org.
[46] M. Solaimanian, T.W. Kennedy, Predicting maximum pavement surface temperature using maximum air temperature and hourly solar radiation, Transportation Research Record. (1993) 1–1.
[47] K. Wang, S. Liang, Global atmospheric downward longwave radiation over land surface under all-sky conditions from 1973 to 2008, Journal of Geophysical Research: Atmospheres. 114 (2009). https://doi.org/10.1029/2009JD011800.
[48] D. Brunt, Notes on radiation in the atmosphere. I, Quarterly Journal of the Royal Meteorological Society. 58 (1932) 389–420.
[49] K. Yang, G.W. Huang, N. Tamai, A hybrid model for estimating global solar radiation, Solar Energy. 70 (2001) 13–22. https://doi.org/10.1016/S0038-092X(00)00121-3.
[50] A. Kotopouleas, R. Giridharan, M. Nikolopoulou, R. Watkins, M. Yeninarcilar, Experimental investigation of the impact of urban fabric on canyon albedo using a 1:10 scaled physical model, Solar Energy. 230 (2021) 449–461. https://doi.org/10.1016/j.solener.2021.09.074.
[51] M. Aida, Urban albedo as a function of the urban structure — A model experiment,

867 Boundary-Layer Meteorol. 23 (1982) 405–413.
868 https://doi.org/10.1007/BF00116269.
869 [52] U. Sievers, W. Zdunkowski, A numerical simulation scheme for the albedo of city
870 street canyons, Boundary-Layer Meteorology. 33 (1985) 245–257.
871 https://doi.org/10.1007/BF00052058.
872 [53] H. Li, J. Harvey, A. Kendall, Field measurement of albedo for different land cover
873 materials and effects on thermal performance, Building and Environment. 59
874 (2013) 536–546. https://doi.org/10.1016/j.buildenv.2012.10.014.
875 [54] Repository of free climate data for building performance simulation.
876 http://climate.onebuilding.org/ (accessed April 9, 2021).
877 [55] E. Andreou, K. Axarli, Investigation of urban canyon microclimate in traditional
878 and contemporary environment. Experimental investigation and parametric
879 analysis, Renewable Energy. 43 (2012) 354–363.
880 https://doi.org/10.1016/j.renene.2011.11.038.
881 [56] N. Mohajeri, A. Gudmundsson, T. Kunckler, G. Upadhyay, D. Assouline, J.H.
882 Kämpf, J.L. Scartezzini, A solar-based sustainable urban design: The effects of
883 city-scale street-canyon geometry on solar access in Geneva, Switzerland, Applied
884 Energy. 240 (2019) 173–190. https://doi.org/10.1016/j.apenergy.2019.02.014.
885 [57] K.K.-L. Lau, C. Ren, J. Ho, E. Ng, Numerical modelling of mean radiant
886 temperature in high-density sub-tropical urban environment, Energy and
887 Buildings. 114 (2016) 80–86. https://doi.org/10.1016/j.enbuild.2015.06.035.
888 [58] F. Ali-Toudert, H. Mayer, Numerical study on the effects of aspect ratio and
889 orientation of an urban street canyon on outdoor thermal comfort in hot and dry
890 climate, Building and Environment. 41 (2006) 94–108.
891 https://doi.org/10.1016/j.buildenv.2005.01.013.
892 [59] V. Lontorfos, C. Efthymiou, M. Santamouris, On the time varying mitigation
893 performance of reflective geoengineering technologies in cities, Renewable
894 Energy. 115 (2018) 926–930. https://doi.org/10.1016/j.renene.2017.09.033.
895 [60] S. Sen, J. Roesler, Aging albedo model for asphalt pavement surfaces, Journal of
896 Cleaner Production. 117 (2016) 169–175.
897 https://doi.org/10.1016/j.jclepro.2016.01.019.
898 [61] I. Pigliautile, M. Chàfer, A.L. Pisello, G. Pérez, L.F. Cabeza, Inter-building
899 assessment of urban heat island mitigation strategies: Field tests and numerical
900 modelling in a simplified-geometry experimental set-up, Renewable Energy. 147
901 (2020) 1663–1675. https://doi.org/10.1016/j.renene.2019.09.082.
902 [62] S. Tsoka, T. Theodosiou, K. Tsikaloudaki, F. Flourentzou, Modeling the
903 performance of cool pavements and the effect of their aging on outdoor surface
904 and air temperatures, Sustainable Cities and Society. 42 (2018) 276–288.
905 https://doi.org/10.1016/j.scs.2018.07.016.
906 [63] M. Santamouris, G.Y. Yun, Recent development and research priorities on cool
907 and super cool materials to mitigate urban heat island, Renewable Energy. 161
908 (2020) 792–807. https://doi.org/10.1016/j.renene.2020.07.109.

[64] C.S. Rowland, R.D. Morton, L. Carrasco, G. McShane, A.W. O'Neil, C.M. Wood, Land Cover Map 2015 (vector, GB), (2017). https://doi.org/10.5285/6c6c9203-7333-4d96-88ab-78925e7a4e73.
[65] T. Holderness, S. Barr, R. Dawson, J. Hall, An evaluation of thermal Earth observation for characterizing urban heatwave event dynamics using the urban heat island intensity metric, International Journal of Remote Sensing. 34 (2013) 864–884. https://doi.org/10.1080/01431161.2012.714505.